

ALTERNATIVE BLUE PIGMENTS WITH HIGH NIR REFLECTANCE TO COBALT BLUE

S. Cerro¹, A. Monrós², M. Llusar¹, V. Esteve¹, G. Monrós¹,

¹Dept. of Inorganic and Organic chemistry, Universidad Jaume I, Castellón (Spain),

²Solar Pigment SL, Espaitec, Universidad Jaume I, Castellón (Spain)

ABSTRACT

The demand for cobalt oxides has risen significantly owing to their indispensable role in lithium batteries and other electronic uses. Although prices increased alarmingly in 2018, they slowed in 2019 owing to a great rise in production in the Congo Republic under socially disrespectful conditions. On the other hand, the REACH regulation classifies Co_3O_4 as a cat. 2 skin sensitising (Ss) and respiratory sensitising (Sr) carcinogen (C). Cobalt is the basis for blue pigment and ceramic ink development. This paper discusses different options, in terms of performance, glaze stability, hazard, and

solar reflectance, for obtaining cobalt-free blue pigments. These involved solid solutions of nickel in willemite ($\text{Ni-Zn}_2\text{SiO}_4$) or hibonite ($\text{Ni-CaAl}_{12}\text{O}_{19}$), those based on the solid solution of strontium in cuprorivaite ($\text{Sr-CaCuSi}_4\text{O}_{10}$) of the Egyptian blue type or doped with rare earths, the solid solution of europium in neodymium oxide ($\text{Eu}^{3+}\text{-Nd}_2\text{O}_3$) and Mn-YInO_3 blue, based on rare earths not classified in the REACH regulation. Cobalt blue in its different varieties (olivine, spinel, or willemite), displayed low NIR reflectance in glazes, on dissolving in tetrahedral coordination with intense absorption in the infrared region. Some pigments, in particular cuprorivaite blue and Mn-YInO_3 blue, exhibited high NIR reflectance, the latter in addition displaying high blue intensities in double-fire frits at low temperature (980°C) comparable to those of Co-willemite.

1. INTRODUCTION

The demand for cobalt oxides has risen significantly owing to their indispensable role in lithium batteries and other electronic uses. Although prices increased alarmingly in 2018, they slowed in 2019 owing to a great rise in production in the Congo Republic under socially disrespectful conditions. On the other hand, the REACH regulation classifies Co_3O_4 as a cat. 2 skin sensitising (Ss) and respiratory sensitising (Sr) carcinogen (C). Cobalt is the basis for blue pigment and ceramic ink development (1).

Buildings are responsible for 40% of energy consumption and 36% of CO_2 emissions in developed countries, according to the Green Building and LEED Core Concepts Guide (U.S. Green Building Council) (2). The state of California prescribes a minimum Solar Reflectivity Index, SRI, of 75% (with a minimum solar reflectance after 3-year ageing of 0.63 and minimum solar emittance of 0.75) (3). On 30 November 2016, the European Commission proposed updating Directive 2012/27/EU relative to energy efficiency, under which all new buildings must have almost zero energy consumption by 31 December 2020. A critical aspect of energy efficiency in climate change strategy, owing to global warming, is the low solar reflectivity of building envelopes as well as of urban public spaces (streets and roads). The overall albedo effect is decreasing, not just because of the loss of snow-covered surface area (owing to climate change), but also the tremendous increase in urbanised (paved) surface with low solar reflectivity (4). Cobalt blue in its different varieties (olivine Co_2SiO_4 , spinel CoAl_2O_4 , or willemite doped with cobalt $\text{Co-Zn}_2\text{SiO}_4$) exhibited low NIR reflectance; the previous structures were not stable in the glazes; and the colour was due to cation Co^{2+} dissolution in tetrahedral coordination in the glazes with intense absorption in the infrared region (5).

2. OBJECTIVES

This paper discusses different options for obtaining cobalt-free blue pigments in terms of performance, glaze stability, hazard, and solar reflectance. These involved solid solutions of nickel in willemite ($\text{Ni-Zn}_2\text{SiO}_4$) (5) or hibonite ($\text{Ni-CaAl}_{12}\text{O}_{19}$) (6), those based on solid solutions of strontium in cuprorivaite ($\text{Sr-CaCuSi}_4\text{O}_{10}$) of the Egyptian blue type or doped with rare earths (7), solid solution of europium in neodymium oxide ($\text{Eu}^{3+}\text{-Nd}_2\text{O}_3$) based on rare earths not classified in the REACH regulation (8) and Mn-YInO_3 blue (9).

3. EXPERIMENTAL

So-called “cool” pigments are pigments with high reflectivity in the near-infrared region (NIR, 780-2100 nm), protecting the building with a highly reflective cladding envelope to infrared rays with interesting environmental benefits, such as significant savings in building thermal conditioning and mitigation of the urban heat island effect (4).

Surface total solar reflectivity (R) is measured by spectrometry using diffuse reflectance UV-Vis-NIR (300-2500 nm) relative to the standard solar spectrum (total fraction of solar energy reflected under previously described standard atmospheric conditions). The solar spectrum used is that of the American Society for Testing and Materials (ASTM G173-03, 2003). This method is used to calculate surface total solar reflectivity, R, from equation 1.

$$R = \frac{\int_{300}^{2500} r(\lambda)i(\lambda)d\lambda}{\int_{300}^{2500} i(\lambda)d\lambda} \text{ (equation 1)}$$

Where $r(\lambda)$ is the spectral reflectance measurement at each wavelength of the studied surface and $i(\lambda)$ is the spectral irradiance at the wavelength considered, in the standard solar spectrum of the American Society for Testing and Materials (ASTM G173-03, 2003) (10).

In this study, the performance of cobalt-doped willemite blue was examined and compared with that of the following blue pigments:

- 1) Solid solution of nickel in willemite ($\text{Ni-Zn}_2\text{SiO}_4$)
- 2) Solid solution of nickel in hibonite ($\text{Ni-CaAl}_{12}\text{O}_{19}$)
- 3) Cuprorivaite ($\text{CaCuSi}_4\text{O}_{10}$) alone or doped with Sr.
- 4) Solid solution of europium in neodymium oxide ($\text{Eu}^{3+}\text{-Nd}_2\text{O}_3$)
- 5) Solid solution of Mn in YInO_3

In the ceramic samples, the precursors, supplied by ALDRICH, with a particle size of 0.3–5 μm , except for ZnO or the quartz used as core in the DPC (dry powder coating) method described below, with a relatively high particle size (1–45 μm), were mixed and mechanically homogenised in an electric grinding mill (20000 rpm) for 5 min. The mixture was fired at the appropriate temperature for the corresponding residence time. The powders were glazed at 5% by weight in monoporosa frit (1080°C) and, in the cases of interest, in a double-fire frit (980°C). The samples were characterised by the following techniques:

- a) The powder samples were characterised by X-ray diffraction of randomly oriented powder in a Siemens D5000 diffractometer with $\text{Cu K}\alpha$ radiation in the range 10–70°2 θ , scan speed 0.05 °2 θ /s, time constant 10 s, and conditions of 40 kV and 20 mA. The powders yielded glazed pieces with glazes at 5% by weight in a double-fire frit (980°C) and monoporosa frit (1080°C).

- b) Colorimetric characterisation of the small glazed slabs was performed by measuring the colour parameters $L^*a^*b^*$ according to the CIE (Commission International de l'Eclairage) methodology, using a Jasco V670 spectrometer, with D65 illuminant and 10° observer. In this method, L^* measures clarity (100=white, 0=black), a^* and b^* measure chroma ($-a^*$ =green, $+a^*$ =red, $-b^*$ =blue, $+b^*$ =yellow) (11).
- c) Surface total solar reflectance (R) was evaluated by spectrometry using UV-Vis-NIR (300–2500 nm) diffuse reflectance relative to the standard solar spectrum, with a Jasco V670 spectrometer of the powder samples and glazed pieces obtained according to the above method.

In the case of the willemite-based pigments doped with cobalt or nickel, in addition to preparation in their stoichiometric form, these were prepared by the decorating technique or DPC (dry powder coating) method. Using this method, it was sought to obtain decorated or core-shell pigments in which a ceramic-based core of high reflectance (e.g. TiO_2 , ZnO) was covered by a layer of pigment. The DPC method has been used to produce special chemicals and ceramics under wet or dry conditions to improve their functionalities. In the dry method, the core, in this case involving high reflectance particles (1–500 μm , for example, ZnO), was mechanically covered with particles, in this case chromophores (0.1–50 μm , Co_3O_4 or NiO), to improve wettability, solubility, and other characteristics, such as reactivity and colour in this case (12). As the host particles are fine, the van der Waals interactions are sufficiently strong to keep them firmly bonded to the core particles. Therefore, discrete or continuous host particle coatings can be obtained depending on the choice of equipment or operating conditions, such as processing time, mechanical action, weight fraction of core host particles, and physical properties of the particles used (13). This discrete or continuous particle coating reacts when it is calcined, generating a shell over the host particle core (e.g. Co_3O_4 and SiO_2 react on coated ZnO particles to yield Ni-doped willemite or $(Zn,Ni)_2SiO_4$).

4. RESULTS and DISCUSSION

4.1. COBALT AND NICKEL WILLEMITES

Figure 1 shows the results obtained for the willemites doped with Co or Ni in their stoichiometric form and by DPC. For the cobalt willemite, ZnO was used as DPC pigment core; for the Ni willemite, quartz was used. Willemite, Zn_2SiO_4 (trigonal, $R\text{-}3H$) with phenakite structure, is an orthosilicate with all atoms in general positions, made up of a structure with tetrahedra accommodating zinc and silicon in three crystallographic positions: two very similar ones for zinc $Zn1$ ($\langle Zn-O \rangle$ 1.950 Å) and $Zn2$ ($\langle Zn-O \rangle$ 1.961 Å), and Si ($\langle Si-O \rangle$ 1.635 Å), yielding a rhombohedral symmetry (14,15).

In powders calcined at 1100°C/3h, cobalt willemite exhibited intense blue colorations (L^* about 38), the blue component b^* being greater in stoichiometric sample W. NIR reflectivity improved 9 points in the DPC sample (37 for W' versus 28 for W).

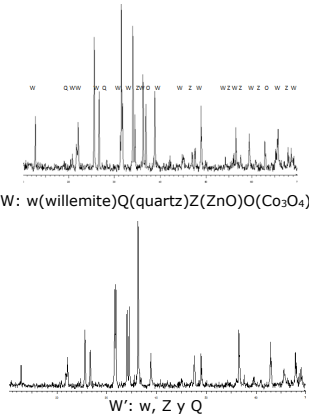
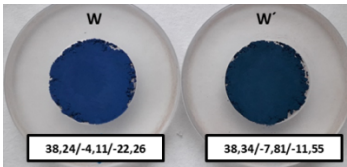
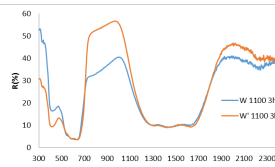
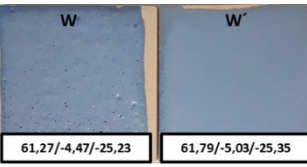
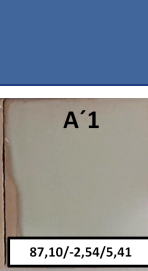
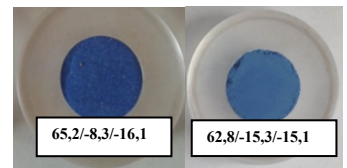
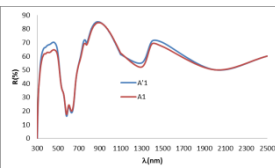
Co-WILLEMITE $\text{Co}_{0,6}\text{Zn}_{1,4}\text{SiO}_4$ 1100°C/3h	W $(\text{Co}_{0,6}\text{Zn}_{1,4})\text{SiO}_4$	W' $(\text{Co}_{0,6}\text{Zn}_{1,4})\text{SiO}_4 \cdot \text{ZnO}$	UV-Vis-NIR spectra	Monoporosa glazes at 5%
 <p>W: w(willemite)Q(quartz)Z(ZnO)O(Co₃O₄)</p> <p>W': w, Z y Q</p>	 <p>W: 38,24/-4,11/-22,26</p> <p>W': 38,34/-7,81/-11,55</p>	 <p>$R_{\text{vis}}/R_{\text{NIR}}/R = 16/28/21$ $16/37/25$</p>	 <p>W: 61,27/-4,47/-25,23</p> <p>W': 61,79/-5,03/-25,35</p> <p>$R_{\text{vis}}/R_{\text{NIR}}/R = 46/53/48$ $46/55/49$</p> <p>Monoporosa frit 1080°C</p>	
Ni-WILLEMITE $\text{Ni}_{0,4}\text{Zn}_{1,6}\text{SiO}_4$ 1100°C/3h	A1 $\text{Ni}_{0,4}\text{Zn}_{1,6}\text{SiO}_4$	A1' $\text{Ni}_{0,4}\text{Zn}_{1,6}\text{SiO}_4 \cdot \text{SiO}_2$	 <p>$R_{\text{vis}}/R_{\text{NIR}}/R = 46/65/53$ $47/64/54$</p>	 <p>A1: 86,85/-3,98/6,31</p> <p>A1': 87,10/-2,54/5,41</p> <p>Monoporosa frit 1080°C</p>
Ni-WILLEMITE $\text{Ni}_{0,4}\text{Zn}_{1,6}\text{SiO}_4$ 1200°C/3h	 <p>A1: 65,2/-8,3/-16,1</p> <p>A1': 62,8/-15,3/-15,1</p>	 <p>$R_{\text{vis}}/R_{\text{NIR}}/R = 37/58/47$ $39/60/50$</p>	 <p>A1: 61,5/7,1/30,6</p> <p>A1': 65,5/7,9/26,9</p> <p>Double-fire frit 980°C</p>	

Figure 1. Results obtained for willemites doped with Co or with Ni in their stoichiometric form and by DPC.

The UV-Vis-NIR spectrum, which was similar in both W and W' samples, was associated with that of $\text{Co}^{2+}(3d^7)$ in tetrahedral coordination (bands centred at 540, 590, and 640 nm of $u_3: {}^4A_2(F) \rightarrow {}^4T_1(P)$ unfolded into three by Jahn–Teller distortion of the tetrahedral vacancies and particularly with the Russel–Saunders spin–orbit L-S u_2 coupling: ${}^4A_2(F) \rightarrow {}^4T_1(F)$ in the NIR region about 1400 nm and $u_1: {}^4A_2(F) \rightarrow {}^4T_2(F)$ (14,15) at 1600 nm, strongly lowering NIR reflectance to values of 28% in W, which increased to 37% in the DPC sample. X-ray diffraction indicated that in the stoichiometric sample, unreacted Co_3O_4 remained, which was associated with the appearance of pinholes in the monoporosa glazes owing to outgassing relating to Co(III) reduction ($\text{Co}_3\text{O}_4 \rightarrow 3\text{CoO} + 1/2\text{O}_2$). In contrast, the DPC sample, which obviously exhibited ZnO used as pigment core, exhibited blue colorations resembling those of sample W with less cobalt and no pinholing defects.

The nickel willemite calcined at 1100°C did not produce a blue colour in the case of stoichiometric sample A1; however, in the DPC sample, confirming the better reactivity of this methodology, it already generated an interesting blue coloration. In both cases, X-ray diffraction indicated the presence of ZnO and/or NiO (both were isomorphs and displayed peaks in overlapping positions), albeit with less intense peaks in the DPC sample: the blue coloration was not stable in the monoporosa frit glaze. At 1200°C, the blue pigment already displayed b^* values about -16, which were comparable with those of the Co willemite albeit with lower intensity (L^* about 60–65). The UV-Vis-NIR spectrum of the Ni-willemite blues matched the spectrum of $\text{Ni}^{2+}(3d^8)$ in tetrahedral coordination (5,16) with a charge transfer band at 270 nm (outside the range in Fig 1) and the bands:

$u_1: {}^3T_1(3F) \rightarrow {}^3T_2(3F)$ intermediate NIR intensity at 1200 nm

$u_2: {}^3T_1(3F) \rightarrow {}^3T_1(3P)$ very weak in the red-NIR region at 770 nm

$u_3: {}^3T_1(3F) \rightarrow {}^3A_2(3F)$ intense in the yellow–red region at 550-650 nm, average 640 nm.

DPC sample A1' reflectance was similar to that of A1, though slightly higher (60 compared to 58%) and much higher than that of the Co-willemite samples (37% in W').

4.2. HIBONITE BLUES

Figure 2 details the results obtained for nickel-doped hibonite as well as for the simplest aluminate, grossite CaAl_4O_7 (17,18). Hibonite ($\text{CaAl}_{12}\text{O}_{19}$) crystallised in a magnetoplumbite lattice (hexagonal, $P63/mmc$, $Z = 2$), with stoichiometric formula generating $\text{A}^{[12]}\text{M1}^{[6]}\text{M2}_2^{[5]}\text{M3}_2^{[4]}\text{M4}_2^{[6]}\text{M5}_6^{[6]}\text{O}_{19}$. Calcium exhibited 12 coordination (position A), while Al^{3+} was distributed in five crystallographic positions: three octahedral ones (M1, M4, and M5), a tetrahedral one (M3), and an unusual trigonal bipyramid (M2) with five coordination. The divalent ions tended to occupy the M3 position, while the small M^{4+} and M^{5+} ions preferentially took up the M4 position. In fact, the magnetoplumbite group contained significant numbers of divalent, tetravalent, and pentavalent ions, a very flexible structure being involved. In the grossite structure CaAl_4O_7 (monoclinic, $C2/c$, $Z=15$) in which Ca^{2+} exhibited 7 coordination with pseudo symmetry $-C_{2v}$ (C_2), Al^{3+} was distributed in two symmetrically independent tetrahedral positions (symmetry C_1) (18,b).

Samples H with 0.12 mole of Ni ($\text{Ni-CaAl}_{12}\text{O}_{19}$) and H' with 0.2 mole of Ni ($\text{Ni-CaAl}_4\text{O}_7$) calcined at $1450^\circ\text{C}/3\text{h}$ were prepared. X-ray diffraction indicated the presence of three phases in the two samples: hibonite (major phase in H), grossite (major phase in H'), and the presence with weak peaks of spinel NiAl_2O_4 in the two samples. The UV-Vis-NIR spectrum of the Ni-hibonite blues, major phase in W, matched the $\text{Ni}^{2+}(3d^8)$ spectrum in tetrahedral coordination with the bands already discussed for Ni-willemite (16), and in addition exhibited a band at 730 nm, presumably related to the ${}^3\text{A}_{2g}(\text{F}) \rightarrow {}^3\text{T}_{1g}(\text{F})$ transition of octahedral Ni^{2+} (19). The UV-Vis-NIR spectrum of the Ni-grossite blue major phases in W' exhibited bands at 380, 500, 600 (broad and intense), 750 in the visible spectrum and at 800, 1100, and 2200 nm in the NIR region associated with the tetrahedral coordination of Ni^{2+} (16), though additional bands appeared at 380, 500, and 750 nm.

The blue colorations of the powders with b^* values about -10 were lower than those of willemite with Co or Ni, also exhibiting a lower intensity than these (L^* about 80–85). Reflectance was similar to that of Ni-willemite (58 for hibonite and 52 for grossite) and much higher than that of the Co-willemite samples (37% in W'). Neither hibonite nor grossite produced colorations in monoporosa glazes.

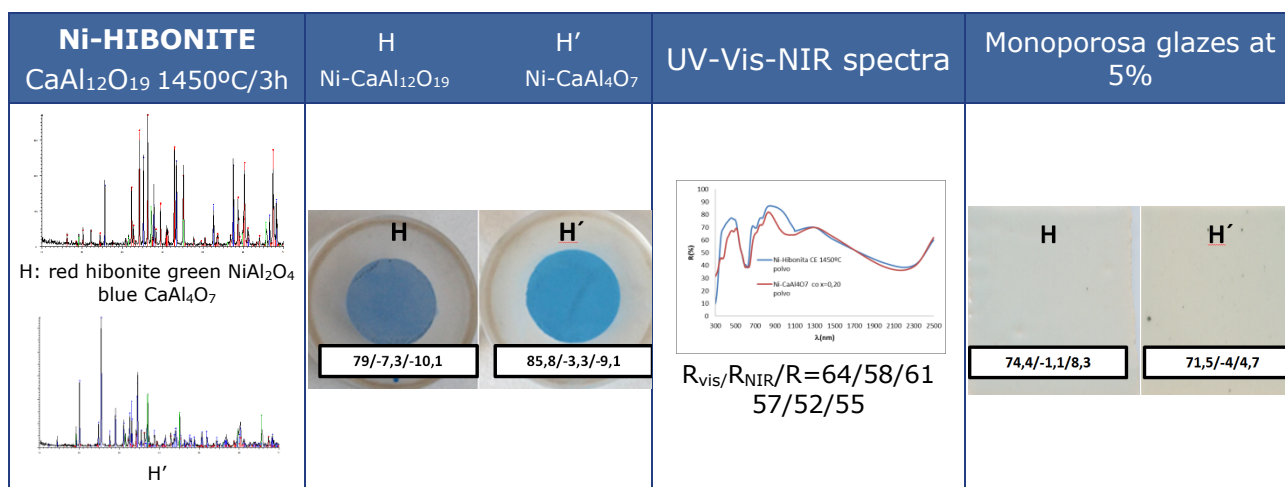


Figure 2. Results obtained for cobalt-free blue pigment.

4.3. CUPRORIVAITE BLUE

Cuprorivaite $\text{CaCuSi}_4\text{O}_{10}$ (tetragonal, $P4/nnc$) is made up of rings of four SiO_4 tetrahedra joined by a copper ion in square-plane coordination forming double layers of copper silicate linked by alkaline earth ions in distorted cube coordination. Figure 2 details the results obtained for cuprorivaite C and for strontium-doped cuprorivaite C'. X-ray diffraction indicated the presence of cuprorivaite as single phase. The UV-Vis-NIR spectra indicated absorption bands (reflectance minima in Fig. 2) at 540, 650, and 800 nm originated by weak d-d transitions of copper (despite symmetry very close to D_{4h} of copper coordination) due to vibronic coupling: that at 800 nm was associated with (${}^2 B_{1g} \rightarrow {}^2 B_{2g}$), that at 650 nm with (${}^2 B_{1g} \rightarrow {}^2 E_g$), and that at 540 nm with (${}^2 B_{1g} \rightarrow {}^2 A_{1g}$) (7,20,21).

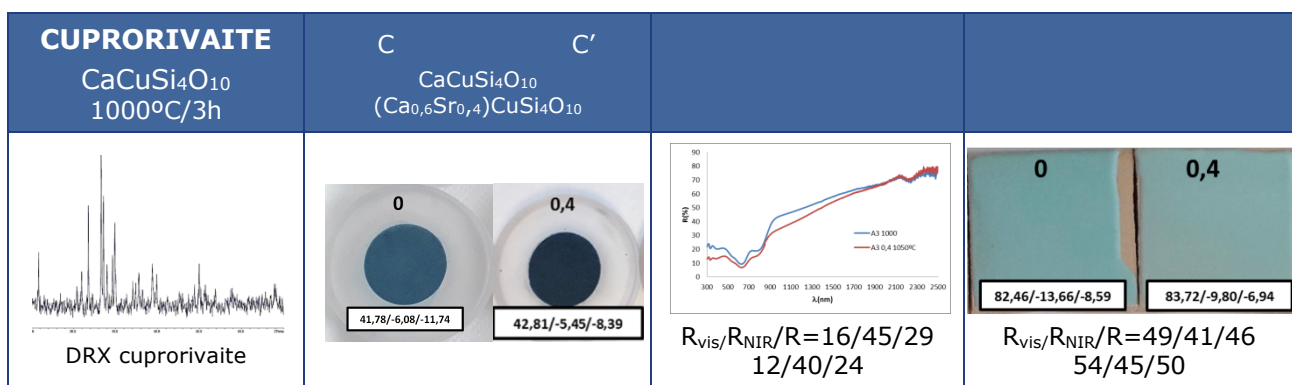


Figure 3. Results obtained for cobalt-free blue pigment.

The blue colorations of the powders with b^* values about -10 were similar to those obtained with hibonite, exhibiting higher intensities than hibonite-grossite (L^* about 42 compared to 80–85 of hibonite-grossite) and comparable to those of the Co willemites ($L^*=38$). The greater NIR reflectance in the non-doped cuprorivaite (45 compared to 40% of the strontium-doped cuprorivaite) was lower than that of Ni-willemite (58 for hibonite and 52 for grossite) but higher than that of the Co-willemite samples (37% in W'). Both non-doped and strontium-doped cuprorivaite produced turquoise colorations in the monoporosa frit glaze with slightly bluer b^* in the non-doped sample (-8.59 versus -6.94 in the doped sample). However, when the powders were calcined at higher temperatures, part of the copper did not enter into solid solution and produced Cu_2O that, on firing, gave rise to pinholes related to outgassing: $\text{Cu}_2\text{O} \rightarrow 2\text{Cu} + 1/2\text{O}_2$ (22).

4.4. EU-ND₂O₃ BLUES

Sesquioxide lanthanides exhibit a hexagonal polymorphism of type A, monoclinic type B, and cubic type C structures, which depends on temperature and on the crystal radius of the Ln³⁺ ion when temperature rises: the metastable form C (IC=6) changes to type A (IC=7), when the crystal radius is relatively high (La-n/a), or to type B (Ic=6-7) when the crystal radius is intermediate (Sm-Gd). Finally, when the crystal radius is low (Tb-Lu), type C is detected as single crystalline polymorph. Neodymium oxide Nd₂O₃ exhibits a type A-based polymorphism which, at low temperatures, displays the metastable phase of the type C Ln₂O₃ structure, whose coordination numbers are 7 and 6 respectively. However, the crystal radius of the Nd³⁺(4f²) ion in an octahedral setting is critical, and a slight decrease in cation radius stabilises the type B structure of M₂O₃ against type A. The effective ionic radii in octahedral environments of Nd³⁺ according to Shannon and Prewitt are 1.123 Å and 1.087 Å¹⁶ for Eu³⁺. If Eu³⁺ replaces the Nd³⁺ ion in the lattice, the average cation radius decreases and can stabilise the type B structure of M₂O₃ against type A. The Nd_{0,9}Eu_{0,1}O₃ composition samples prepared from oxides required high temperatures to stabilise type A Nd₂O₃. However, using the coprecipitation route with halides, at 1200°C this phase stabilised, displaying a blue coloration not attained by conventional glazes in tile production and exhibiting a level of coloration of L*a*b*=79/0/-12 in a monoporosa glaze at 5% (23).

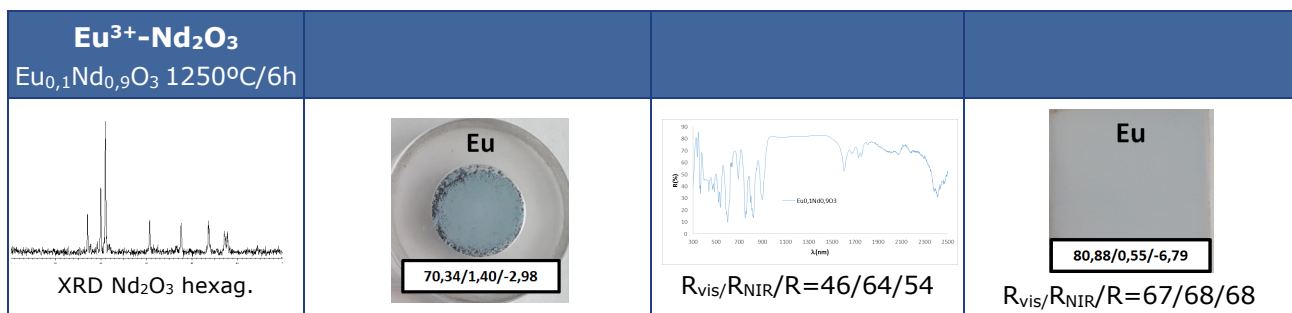


Figure 4. Results obtained for cobalt-free blue pigment.

Figure 4 shows the results of a ceramic sample calcined at 1250°C/6h, in which the type A form (hexagonal, *P-3m1*, Z=164) was detected. The powders exhibited a blue coloration (b*=-2.98) and low intensity (L*=70.3) with high NIR reflectance (64%); in the monoporosa glaze they generated blue (b*=-6.8) and high NIR reflectance (68%). The UV-Vis-NIR spectrum indicated the numerous and relatively low-intensity bands associated with the rare earths (Eu³⁺ and Nd³⁺) involved, which enabled generally high reflectivity. Comparison of this blue with the previous ones, even considering its improvement using non-conventional methods such as coprecipitation, showed that a lighter blue powder was involved than that obtained with Ni-willemite, hibonite, or cuprorivaite and even more in respect of Co-willemite. However, it kept the blue component in the monoporosa glaze, unlike Ni-willemite or hibonite, with values similar to those of cuprorivaite.

4.5. Mn-YInO₃ BLUES

By calcination at 1200°C of the oxide mixture (ceramic route with or without pelletising), Smith et al. (9,25) developed an intense blue pigment based on solid solution of manganese in YInO₃ (the best blue was the stoichiometry YIn_{0.8}Mn_{0.2}O₃ with L*a*b*=34.1/11.7/-44.4 and R=34%, R65=65% in powder and in vinyl paint at 20% 77.9/-2.9/-19.3 con and R(NIR)=62%. The patent protecting the pigment (26) indicates that it can be applied in glasses and ceramics; however, it provides no data on these applications, though it does on cement and vinyl paint.

Figure 5 shows the results obtained in the solid solution YIn_{0.8}Mn_{0.2}O₃ blue and YInO₃ black. X-ray diffraction indicated the presence of YInO₃ as single phase in the former and of MnYO₃ in the latter, both hexagonal, P63cm, Z=185. The almost black sample MnYO₃ was in fact a very dark (L*=27.73) blue (b*=-3.47) with high NIR reflectance for a black colour (39%); both in single-fired glazes at 980°C (black colorations) and in monoporosa glazes (grey colorations) the phase decomposed and produced widespread pinholes, probably related to outgassing of the reduction of Mn³⁺ to Mn²⁺ (Mn₂O₃→2MnO+1/2O₂). The solid solution YIn_{0.8}Mn_{0.2}O₃ gave rise to powders with an intense blue coloration (b*=-39.15) and also with an intense yield (L*=31.84), and at 72% NIR reflectance exceeded all the previous powders including Co-willemite. The UV-Vis-NIR spectrum of the powders indicated strong absorptions (reflectance minima) in all the visible spectrum associated with the Mn³⁺ trigonal plane that had practically no NIR absorption, allowing high reflectances. The monoporosa glaze generated soft blues with L*=-15.43 and L*=66.84 below those obtained with Co-willemite; in contrast, the 79% NIR reflectance was higher in the double-fire frit at low temperature (980°C). The blue was intense L*a*b*=22.16/-3.79/-45.22 exceeding that of Co-willemite, and reflectivity was 71%, making this blue pigment an excellent substitute for use in low-temperature paints and glazes.

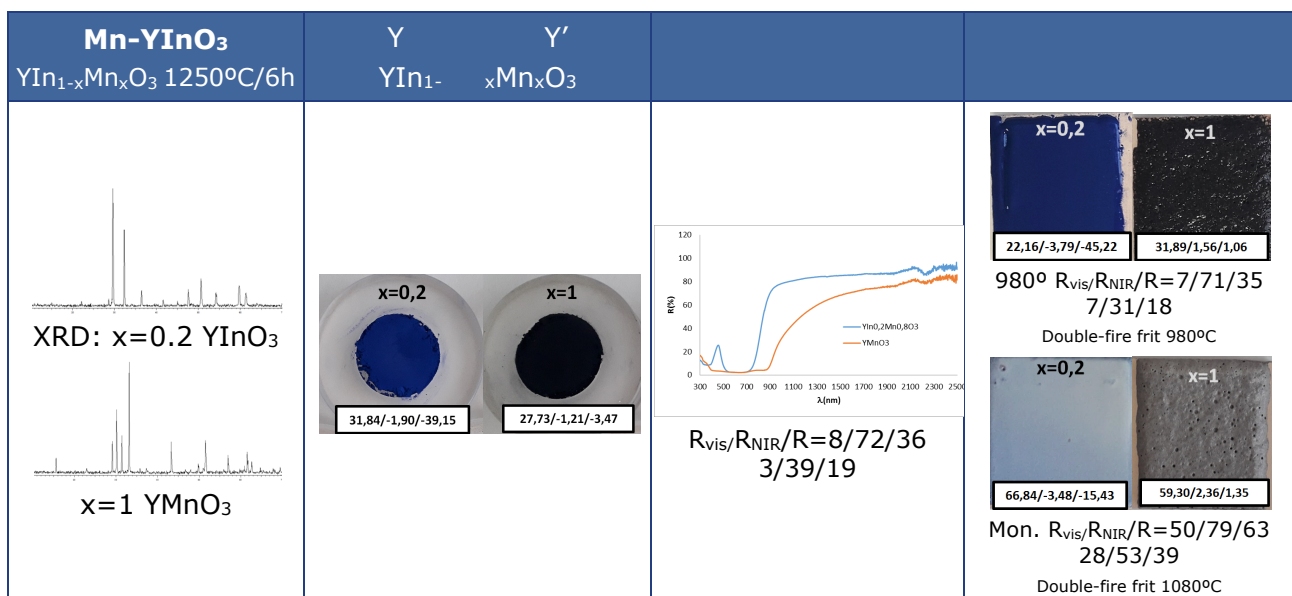


Figure 5. Results obtained for cobalt-free blue pigment.

5. CONCLUSIONS

The following blue pigments were studied as alternatives to Co-willemite: (1) solid solution of nickel in willemite ($\text{Ni-Zn}_2\text{SiO}_4$); (2) solid solution of nickel in hibonite ($\text{Ni-CaAl}_{12}\text{O}_{19}$); (3) cuprorivaite ($\text{CaCuSi}_4\text{O}_{10}$) alone or doped with Sr; (4) solid solution of europium in neodymium oxide ($\text{Eu}^{3+}\text{-Nd}_2\text{O}_3$); and (5) solid solution of Mn in YInO_3 . The blue powders obtained with cuprorivaite and Mn- YInO_3 exhibited better NIR reflectances and were comparable in intensity to the Co-willemite powders used as references; those of hibonite, Ni-willemite, and $\text{Eu}^{3+}\text{-Nd}_2\text{O}_3$ were turquoise and less intense. In applications with monoporous glazes only cuprorivaite and Mn- YInO_3 kept blue tones, though they were less intense than Co-willemite. However, Mn- YInO_3 produced intense blue colorations in single-fired glazes at low temperature (980°C) and very high NIR reflectance.

6. REFERENCES

- [1] D. Gardini, M. Dondi, A. L. Costa, F. Matteucci, M. Blosi, C. Galassi, G. Baldi, and E. Cinotti, Nano-sized ceramic inks for drop-on-demand ink-jet printing in quadrichromy, *Journal of Nanoscience and Nanotechnology*, 8 (2008)1979-1988.
- [2] Altomonte S., Schiavon S., Occupant satisfaction in LEED and non-LEED certified buildings. *Building and Environment* 68 (2013), 66-76.
- [3] California Building Energy Efficiency Standards (Title 24, Part 6) <http://coolroofs.org/resources/california-title-24>.
- [4] (a) G. Monrós, M. Llusar, S. Cerro, Pigmentos termosolares ecoeficientes, Ed. Academica Española, 2017, ISBN 978-620-2-25178-5.
- [5] <https://www.morebooks.de/es/search?utf8=%E2%9C%93&q=Pigmentos+termosolares+e+coeficientes>. (b) G. Monrós, C. Gargori, V. Esteve, M. Llusar, Jaume I University, Spanish Pat. ES 2616347 A1, 2018.
- [6] M. Llusar, A. Monrós, S. Cerro, C. Gargori, G. Monrós, New generations of pigments for the thermal efficiency of buildings, XV World Congress on Ceramic Tile Quality, QUALICER'18, Castellón 2018, *Book of Abstracts*. ISBN:13 978-84-95931-39-9.
- [7] Forés, A., Llusar, M., Badenes, J. A., Calbo, J., Tena, M. and Monrós G., Alternative turquoise blue pigment for glazes. *Am. Ceram. Soc. Bull.*, 2001, **80**, 47-52.
- [8] Costa G.; Hajjaji W.; Seabra, M. P.; Labrincha J. A.; Dondi, Cruciani G., M Ni-doped Hibonite ($\text{CaAl}_{12}\text{O}_{19}$), A New Turquoise Blue Ceramic Pigment, *J. of the European Ceramic Society*, 29,13(2009)2671-2678.
- [9] E. Kendrick, C.J. Kirk CJ, S.E. Dann, Structure and colour properties in the Egyptian Blue Family, $\text{M}_{1-x}\text{M}'_x\text{CuSi}_4\text{O}_{10}$, as a function of M, M' where M, M'=Ca, Sr and Ba. *Dyes Pigm* 73 (2007) 13-18.
- [10] A. García, M. Llusar, S. Sorlí, M. A. Tena, J. Calbo, G. Monrós, $\text{Eu}^{3+}\text{-Nd}_2\text{O}_3$ blue pigmented solid solutions, *British Ceramic transactions*, , 101,6 (2002) 242-246, doi.org/10.1179/096797802225008078.
- [11] A.E. Smith, H. Mizoguchi, K. Delaney, N.A. Spaldin, A.W. Sleight, M.A. Subramanian, Mn^{3+} in trigonal bipyramidal coordination: a new blue chromophore, *J. Am. Chem. Soc.* 131 (2009) 17084-17086.
- [12] Hashem Akbari and Ronnen Levinson, Evolution of Cool-Roof Standards in the US, *Advances in Building Energy Research*, 2(2008)1-32.
- [13] CIE Commission International de l'Eclairage, Recommendations on Uniform Color Spaces, Color Difference Equations, Psychometrics Color Terms. Supplement nº 2 of CIE Pub. Nº 15 (E1-1.31) 1971, Bureau Central de la CIE, Paris (1978).
- [14] R. Pfeffer, R.N. Dave, W. Dongguang, M. Ramlakhan, Synthesis of engineered particulates with tailored properties using dry particle coating, *Powder Technol* 2001:117:40-67
- [15] Y. Ouabbas, A. Chamayou, L. Galet, M. Baron, G. Thomas, P. Grosseau, B. Guilhot, Surface modification of silica particles by dry coating: Characterization and powder ageing, *Powder Technol* 2009:190:200-209.

- [16] A. Forés, M. Llusar, J. A. Badenes, J. Calbo, M. A. Tena, and G. Monrós, "Cobalt minimisation in willemite ($\text{Co}_x\text{Zn}_{2-x}\text{SiO}_4$) ceramic pigments," *Green Chem.*, **2**, 93–100 (2000).
- [17] Llusar M, Forés A, Badenes JA, Calbo J, Tena MA, Monrós G. Colour analysis of some cobalt-based pigments, *J Eur Ceram Soc* 2001;21:1121–30.
- [18] G. Lorenzi, G. Baldi, F. Di Benedetto, V. Faso, P. Lattanzi, M. Romanelli, "Spectroscopic study of a Ni-bearing gahnite pigment", *Journal of the European Ceramic Society* 26 (2006) 317-321.
- [19] (a) Weber, D. and A. Bischoff, Grossite (CaAl_4O_7) – a rare phase in terrestrial rocks and meteorites. *Eur. J. Mineral.*, 6 (1994) 591–594, (b) A. M. HOFMEISTER, B. WOPENKA, A. J. LOCOCK, Spectroscopy and structure of hibonite, grossite, and CaAl_2O_4 : Implications for astronomical environments, *Geochimica et Cosmochimica Acta*, Vol. 68, No. 21, pp. 4485-4503, 2004.
- [20] Jun Li, Elena A. Medina, Judith K. Stalick, Arthur W. Sleight, M.A. Subramanian, [Colored oxides with hibonite structure: a potential route to non-cobalt blue pigments](#), *Progress in Solid State Chemistry*, 44, 4 (2016) 107-122.
- [21] Robert Ianos, Paul Barvinschi, Characterization of $\text{Mg}_{1-x}\text{Ni}_x\text{Al}_2\text{O}_4$ solid solutions prepared by combustion synthesis, *Journal of the European Ceramic Society* 31 (2011) 739–743.
- [22] G. Pozza, D. Ajò, G. Chiari, F. De Zuane, M. Favaro, Photoluminescence of the inorganic pigments Egyptian blue, Han blue and Han purple. *J Cult Heritage* 2000;1:393-398.
- [23] Paul Berdahl, Simon K. Boocock, George C.-Y. Chan, Sharon S. Chen, Ronnen M. Levinson, and Michael A. Zalich, High quantum yield of the Egyptian blue family of infrared phosphors ($\text{MCuSi}_4\text{O}_{10}$, M = Ca, Sr, Ba), *Journal of Applied Physics* 123 (2018)193103.
- [24] S. Cerro, M. Llusar, A. Monrós, V. Esteve, G. Monrós, Pigmentos azules de cuprorivaita de alta reflectancia NIR obtenidos por métodos coloidales, *Qualicer 2020*.
- [25] G. Monrós, El color de la cerámica: nuevos mecanismos en pigmentos para los nuevos procesados en la industria cerámica, Vol I. Castellón, Publicacions de la Universitat Jaume I, 2003.
- [26] M. Llusar, A. Monrós, S. Cerro, C. Gargori, G. Monrós, New generations of pigments for the thermal efficiency of buildings, XV World Congress on Ceramic Tile Quality, QUALICER'18, Castellón 2018, *Book of Abstracts*. ISBN:13 978-84-95931-39-9.
- [27] Materials with trigonal bipyramidal coordination and methods of making the same, US Patent 8,282,728 B2.

7. ACKNOWLEDGEMENTS:

The authors thank Universitat Jaume I (Project UJI-B2018-43) for funding.